Couette and Poiseuille microflows: Analytical solutions for regularized 13-moment equations

Peyman Taheri,[1,a)] Manuel Torrilhon,[2,b)] and Henning Struchtrup[1,c)]
[1]*Department of Mechanical Engineering, University of Victoria, P.O. Box STN CSC 3055, Victoria, British Columbia V8W 3P6, Canada*
[2]*Seminar for Applied Mathematics, ETH Zurich, ETH-Zentrum, CH-8092 Zurich, Switzerland*

(Received 13 June 2008; accepted 18 November 2008; published online 28 January 2009)

The regularized 13-moment equations for rarefied gas flows are considered for planar microchannel flows. The governing equations and corresponding kinetic boundary conditions are partly linearized, such that analytical solutions become feasible. The nonlinear terms include contributions of the shear stress and shear rate, which describe the coupling between velocity and temperature fields. Solutions for Couette and force-driven Poiseuille flows show good agreement with direct simulation Monte Carlo data. Typical rarefaction effects, e.g., heat flux parallel to the wall and the characteristic dip in the temperature profile in Poiseuille flow, are reproduced accurately. Furthermore, boundary effects such as velocity slip, temperature jump, and Knudsen boundary layers are predicted correctly. © *2009 American Institute of Physics*. [DOI: 10.1063/1.3064123]

I. INTRODUCTION

It is well known that the classical Navier–Stokes–Fourier equations fail to describe flows in rarefied gases.[1] This shortcoming of classical hydrodynamics is due to nonequilibrium behavior of the gas on length scales of the order of the mean free path, e.g., in miniaturized and/or low-pressure devices, where the Knudsen number (Kn) is not small. Such rarefied conditions are common in microelectromechanical systems, microfluidic devices, porous media, biomedical assemblies, high-altitude flights, and vacuuming instruments.

The fundamental problems of rarefied Couette and Poiseuille flows in planar geometry have been investigated from different perspectives. Now, it is well established that a wealth of nonequilibrium effects exists in dilute Couette and Poiseuille flows, which the Navier–Stokes–Fourier theory cannot describe. Heat flux parallel to flow direction which is not forced by temperature gradient,[2–6] nonuniform pressure profile,[5–9] and characteristic temperature dip in Poiseuille flow[6–13] are among the most prominent effects. Moreover, in rarefied flows, the formation of Knudsen boundary layers affects the bulk solution[14–16] and the so-called Knudsen minimum[17] can only be captured with second-order slip condition on the walls.[16–21]

The dynamics of dilute gases is perfectly described by the Boltzmann equation. The numerical or analytical solution of the Boltzmann equation is rather involved, and thus, in practice, computational difficulties still remain as the major problem in direct application of the Boltzmann equation. The most successful method for the solution of the Boltzmann equation is the direct simulation Monte Carlo method (DSMC),[22] which, however, leads to stochastic noise, in particular, for microflows, where the Mach number is small; moreover it requires particularly large numerical effort for unsteady problems. Several techniques have been presented to simplify the Boltzmann equation while retaining accuracy. Macroscopic models[1] and lattice Boltzmann (LB) models[23,24] are among the most popular approaches.

Approximation methods in kinetic theory[1] derive macroscopic transport equations from the Boltzmann equation at different levels of accuracy. The Chapman–Enskog method[25] is the classical approach to derive constitutive equations for heat flux and shear by means of an expansion in the Knudsen number. In the Chapman–Enskog method, the Euler and Navier–Stokes–Fourier equations follow from the zeroth-order and first-order expansions, and the second- and third-order expansions lead to the Burnett and super-Burnett equations, respectively. The severe disadvantage of the classical Burnett and super-Burnett equations is their linear instability.[26,27] Several papers have been devoted to this problem, and authors have suggested different techniques to stabilize the equations, including the augmented Burnett equations,[28] the regularized Burnett equations,[29] consistently ordered extended thermodynamics,[30] hyperbolic Burnett equations,[31] and hybrid Burnett equations.[32]

Recently, it was shown[33,34] that inclusion of high-order moments in isothermal LB methods and increasing the number of discrete velocities can shift the ability of LB methods beyond the hydrodynamics regime. Nevertheless, LB methods are still vulnerable to instabilities when temperature-dependent calculations are required.

Grad's moment method[35,36] is another competent approach to derive macroscopic models from the Boltzmann equation. In the present work, we focus on a recently developed macroscopic model, the regularized 13 (R13)-moment equations, which are an extension of Grad's well-known set of 13-moment equations. The idea of regularization goes back to Grad[36] and was later revived by Karlin *et al.*,[37] who derived a set of linear transport equations but did not provide

[a)]Electronic mail: peymant@uvic.ca.
[b)]Electronic mail: matorril@math.ethz.ch.
[c)]Electronic mail: struchtr@uvic.ca.

numerical values for the various transport coefficients. The complete set of the R13-moment equations was derived in Refs. 38 and 39. The R13 equations are appropriate for rarefied flows up to the transition regime, i.e., $\mathrm{Kn}<1$, and provide a stable set of transport equations of super-Burnett order, $\mathcal{O}(\mathrm{Kn}^3)$. Furthermore, they generate continuous shock structures at all Mach numbers[40] and capture Knudsen boundary layers[38,41] as well. Thus, they cover the whole spectrum of flow between the linear regime, where effects such as Knudsen layers dominate, and the nonlinear regime, where nonlinear bulk effects and shocks become important. With these features the R13 equations are, at present, the most promising macroscopic model for rarefied gas flows.[42]

For a long time, the nonavailability of proper boundary conditions for high-order moments was the major obstacle in rendering the R13 equations and any other set of extended equations including the various forms of the Burnett equations into an engineering tool. Only recently, building up on Grad's discussion of the problem,[35,36] boundary conditions for the R13 equations were derived from the boundary conditions of the Boltzmann equation by Gu and Emerson[43] and by Torrilhon and Struchtrup.[44] The kinetic boundary conditions proposed by Gu and Emerson show spurious boundary layers, probably due to prescription of more boundary conditions than mathematically required. Torrilhon and Struchtrup checked both physical and mathematical consistencies of their boundary conditions on Couette and Poiseuille flows within microchannels. Their numerical solutions show excellent agreement with the DSMC simulations.[44] Using the principles of classical nonequilibrium thermodynamics, it was shown that the linearized R13 equations and their boundary conditions lead to positive entropy production, i.e., the H theorem is fulfilled both for the gas and the gas-wall interface.[45]

In the present paper, we consider a semilinearized form of the R13 system, with semilinearized boundary conditions, that provides analytical solutions for classical flows. The nonlinear terms describe the irreversible coupling between the fields of temperature and velocity, which is not accessible to the LB equations of Refs. 33 and 34. This simplified approach leads to outstanding agreement with the DSMC data and gives further evidence of the reliability of the R13 system and also supports the theory behind the development of boundary conditions. Indeed, the most remarkable feature of the presented approach is its accuracy and robustnes and a rather rich array of rarefaction effects, which can be achieved without complicated numerical schemes. Moreover, the analytical solutions allow to obtain deeper insight into rarefaction effects, such as heat flux parallel to the wall and the characteristic dip in the temperature profile which is observed in force-driven Poiseuille flow.[11,12,46]

II. R13 EQUATIONS

We first present the full nonlinear R13 system.[39] The first five equations are the conservation laws for mass, momentum, and energy,

$$\frac{D\rho}{Dt}+\rho\frac{\partial v_k}{\partial x_k}=0,$$

$$\rho\frac{Dv_i}{Dt}+\frac{\partial p_{ik}}{\partial x_k}=\rho G_i, \tag{1}$$

$$\rho\frac{De}{Dt}+\frac{\partial(p_{ik}v_i+q_k)}{\partial x_k}=\rho G_i v_i,$$

where t and x_k represent independent variables, i.e., time and spatial position. Moreover, ρ, v_k, p_{ik}, e, G_i, and q_k denote mass density, velocity, pressure tensor, (total) energy density, body force, and heat flux, with

$$p_{ik}=p\delta_{ik}+\sigma_{ik} \quad \text{and} \quad e=u+\tfrac{1}{2}v^2. \tag{2}$$

Here, u stands for internal energy density, and p and σ_{ij} are the pressure and stress tensor (nonequilibrium part of the pressure tensor); the stress tensor σ_{ij} is symmetric and trace-free. Since we consider ideal monatomic gases, $p=\rho\theta$ and $u=\frac{3}{2}\theta$ hold as the equations of state, where θ is the temperature in energy units ($\theta=RT$ where R is the gas constant and T is the thermodynamic temperature). The convective derivative is defined as $D/Dt=\partial/\partial t+v_k(\partial/\partial x_k)$.

In the R13 system, the equations for heat-flux vector and stress tensor are their respective moment equations,[1,35,36,38,39] i.e.,

$$\begin{aligned}\frac{Dq_i}{Dt}&+\underline{\frac{5}{2}\rho\theta\frac{\partial\theta}{\partial x_i}}-\sigma_{ik}\theta\frac{\partial\ln\rho}{\partial x_k}-\frac{\sigma_{ij}}{\rho}\frac{\partial\sigma_{jk}}{\partial x_k}+\frac{5}{2}\sigma_{ik}\frac{\partial\theta}{\partial x_k}\\&+\theta\frac{\partial\sigma_{ik}}{\partial x_k}+\frac{7}{5}q_k\frac{\partial v_i}{\partial x_k}+\frac{7}{5}q_i\frac{\partial v_k}{\partial x_k}+\frac{2}{5}q_k\frac{\partial v_k}{\partial x_i}+\frac{1}{2}\frac{\partial R_{ik}}{\partial x_k}\\&+\frac{1}{6}\frac{\partial\Delta}{\partial x_i}+m_{ijk}\frac{\partial v_j}{\partial x_k}=-\underline{\frac{2}{3}\frac{p}{\mu}}q_i,\end{aligned} \tag{3}$$

and

$$\begin{aligned}\frac{D\sigma_{ij}}{Dt}&+\sigma_{ij}\frac{\partial v_k}{\partial x_k}+\frac{4}{5}\frac{\partial q_{\langle i}}{\partial x_{j\rangle}}+\underline{2\rho\theta\frac{\partial v_{\langle i}}{\partial x_{j\rangle}}}+2\sigma_{k\langle i}\frac{\partial v_{j\rangle}}{\partial x_k}+\frac{\partial m_{ijk}}{\partial x_k}\\&=-\underline{\frac{p}{\mu}}\sigma_{ij},\end{aligned} \tag{4}$$

where μ denotes viscosity and the indices inside angular brackets indicate trace-free symmetric tensors.

The 13-moment equations (1), (3), and (4) contain the additional higher moments Δ, R_{ik}, and m_{ijk}. In Grad's classical 13-moment theory[35,36] these vanish, $\Delta=R_{ik}=m_{ijk}=0$, while the regularization procedure gives[1,38,39]

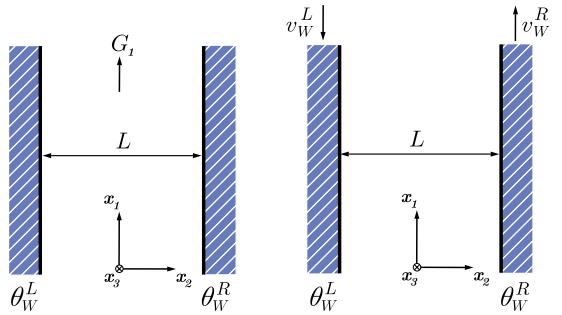

FIG. 1. (Color online) Poiseuille flow (left) and Couette flow (right): In force-driven Poiseuille flow, the gas is driven through the action of body forces G_i. In Couette flow, the walls of the channel are moving, and the gas moves as the result of shear stress diffusion from the walls.

$$\Delta = -\frac{\sigma_{ij}\sigma_{ij}}{\rho} - 12\frac{\mu}{p} \times\left(\theta\frac{\partial q_k}{\partial x_k} + \frac{5}{2}q_k\frac{\partial\theta}{\partial x_k} - \theta q_k\frac{\partial \ln\rho}{\partial x_k} + \theta\sigma_{kl}\frac{\partial v_k}{\partial x_l}\right),$$

$$R_{ij} = -\frac{4}{7}\frac{\sigma_{k\langle i}\,\sigma_{\,j\rangle k}}{\rho} - \frac{24}{5}\frac{\mu}{p} \times\left(\theta\frac{\partial q_{\langle i}}{\partial x_{\,j\rangle}} + q_{\langle i}\frac{\partial\theta}{\partial x_{\,j\rangle}} - \theta q_{\langle i}\frac{\partial \ln\rho}{\partial x_{\,j\rangle}} + \frac{10}{7}\theta\sigma_{k\langle i}S_{\,j\rangle k}\right), \quad (5)$$

$$m_{ijk} = -2\frac{\mu}{p}\left(\theta\frac{\partial\sigma_{\langle ij}}{\partial x_{\,k\rangle}} - \theta\sigma_{\langle ij}\frac{\partial \ln\rho}{\partial x_{\,k\rangle}} + \frac{4}{5}q_{\langle i}\frac{\partial v_{\,j}}{\partial x_{\,k\rangle}}\right),$$

with $S_{jk}=\partial v_{\langle j}/\partial x_{\,k\rangle}$.

In the limit of small Knudsen numbers Eqs. (3) and (4) reduce to Fourier's law, $q_i=-(15/4)\mu(\partial\theta/\partial x_i)$, and Navier–Stokes law, $\sigma_{ij}=-2\mu(\partial v_{\langle i}/\partial x_{\,j\rangle})$ (only the underlined terms remain in the equations).[1,38]

III. PROBLEM STATEMENT

Classical internal flows, namely, Couette and force-driven Poiseuille flows, are chosen to investigate the most important rarefaction effects, e.g., temperature jump, velocity slip, and formation of Knudsen boundary layers.

We assume steady state flows confined between two infinite planar parallel plates, see Fig. 1, where velocity, temperature, and all other flow parameters are independent of the flow direction x_1. The impermeable walls act as thermal reservoirs, and the velocity normal to the walls, v_2, is zero. These conditions give

$$\frac{D}{Dt} = \frac{\partial}{\partial t} + v_k\frac{\partial}{\partial x_k} = 0, \quad v_i = \{v(x_2),0,0\}, \quad \frac{\partial v_k}{\partial x_k} = 0. \quad (6)$$

Since these two-dimensional flow settings are independent of the direction x_3, stress tensor and heat-flux vector reduce to

$$\sigma_{ij} = \begin{bmatrix} \sigma_{11}(x_2) & \sigma_{12}(x_2) & 0 \\ \sigma_{12}(x_2) & \sigma_{22}(x_2) & 0 \\ 0 & 0 & -\sigma_{11}(x_2)-\sigma_{22}(x_2) \end{bmatrix},$$
$$q_i = \{q_1(x_2), q_2(x_2), 0\}, \quad (7)$$

where all components depend solely on x_2. Indeed, q_1 remains among the variables because gas particles travel in all directions, so through the collisions they can transfer energy to all directions. It is worth mentioning that nonvanishing q_1 lies outside the hydrodynamic regime—the classical Navier–Stokes–Fourier equations give heat flux only in the direction of the temperature gradient and cannot predict the tangential heat flux q_1, which is not driven by a temperature gradient.

As depicted in Fig. 1, the channel walls are parallel in direction x_1 at constant distance L. The walls are located on $x_2=\pm(L/2)$ and maintained at constant temperatures θ_W^L and θ_W^R. In the case of Poiseuille flow, the channel walls are stationary, and the gas is driven by an external body force G_1. In Couette flow there is no body force, but the walls move with velocities $v_W^L=-v_W$ and $v_W^R=+v_W$ relative to the center.

IV. SEMILINEARIZED AND DIMENSIONLESS R13 EQUATIONS FOR CHANNEL FLOWS

A. The equations

Nondimensionalization and partial linearization are performed with respect to a reference equilibrium state, defined by $\{\rho_0,\theta_0,v_i^0=0\}$. In standard linearization only terms that are linear in deviations from the ground state are considered, which removes viscous heating from the energy balance. However, flow field and temperature are coupled through the viscous heating term $-\sigma_{ij}(\partial v_i/\partial x_j)$, which is nonlinear. To retain this coupling in the equations, we considered semilinearization, such that all nonlinear terms are removed except those which introduce quadratic contributions of the shear stress σ_{12}, shear rate dv_1/dx_2, and their combinations (including higher derivatives).

In order to provide a clear discussion on the relevant nonlinear contributions in the semilinearized equations, we first present the fully nonlinear R13 equations in dimensionless form for the suggested flow geometry. For detailed information about the dimensionless parameters see the Appendix. Equations (1)–(5) are simplified with respect to the prescribed flow conditions (6) and (7). Consequently, the conservation laws for mass and momentum in direction x_3 vanish. In the same fashion, the balance equation for the heat-flux vector, Eq. (3), leads to a trivial equation for q_3. Since the stress tensor is symmetric and trace-free, five balance equations for $\{\sigma_{11},\sigma_{12},\sigma_{13},\sigma_{22},\sigma_{23}\}$ are required, but due to the geometry, the equations for σ_{13} and σ_{23} turn out to be trivial.

The obtained equations can be presented as the following set of ordinary differential equations:

$$\frac{d\sigma_{12}}{dx_2} = \rho G_1, \tag{8}$$

$$\frac{d(\rho\theta + \sigma_{22})}{dx_2} = 0, \tag{9}$$

$$\frac{dq_2}{dx_2} = -\sigma_{12}\frac{dv_1}{dx_2}, \tag{10}$$

$$-\frac{4}{15}\frac{dq_2}{dx_2} + \frac{4}{3}\sigma_{12}\frac{dv_1}{dx_2} + \frac{dm_{112}}{dx_2} = -\frac{1}{\mathrm{Kn}_0}\frac{p}{\mu}\sigma_{11}, \tag{11}$$

$$\frac{2}{5}\frac{dq_1}{dx_2} + \rho\theta\frac{dv_1}{dx_2} + \underline{\sigma_{22}\frac{dv_1}{dx_2}} + \frac{dm_{122}}{dx_2} = -\frac{1}{\mathrm{Kn}_0}\frac{p}{\mu}\sigma_{12}, \tag{12}$$

$$\frac{8}{15}\frac{dq_2}{dx_2} - \frac{2}{3}\sigma_{12}\frac{dv_1}{dx_2} + \frac{dm_{222}}{dx_2} = -\frac{1}{\mathrm{Kn}_0}\frac{p}{\mu}\sigma_{22}, \tag{13}$$

$$\underline{-\sigma_{12}\theta\frac{d\ln\rho}{dx_2}} - \underline{\frac{\sigma_{11}}{\rho}\frac{d\sigma_{12}}{dx_2}} - \underline{\frac{\sigma_{12}}{\rho}\frac{d\sigma_{22}}{dx_2}} + \underline{\frac{5}{2}\sigma_{12}\frac{d\theta}{dx_2}} + \theta\frac{d\sigma_{12}}{dx_2} + \underline{\frac{7}{5}q_2\frac{dv_1}{dx_2}} + \frac{1}{2}\frac{dR_{12}}{dx_2} + \underline{m_{112}\frac{dv_1}{dx_2}} = -\frac{2}{3}\frac{1}{\mathrm{Kn}_0}\frac{p}{\mu}q_1, \tag{14}$$

$$\frac{5}{2}\rho\theta\frac{d\theta}{dx_2} - \underline{\sigma_{22}\theta\frac{d\ln\rho}{dx_2}} - \frac{\sigma_{12}}{\rho}\frac{d\sigma_{12}}{dx_2} - \underline{\frac{\sigma_{22}}{\rho}\frac{d\sigma_{22}}{dx_2}} + \underline{\frac{5}{2}\sigma_{22}\frac{d\theta}{dx_2}} + \theta\frac{d\sigma_{22}}{dx_2} + \frac{2}{5}q_1\frac{dv_1}{dx_2} + \frac{1}{2}\frac{dR_{22}}{dx_2} + \frac{1}{6}\frac{d\Delta}{dx_2} + m_{122}\frac{dv_1}{dx_2} = -\frac{2}{3}\frac{1}{\mathrm{Kn}_0}\frac{p}{\mu}q_2. \tag{15}$$

The constitutive parameters which appear in the above equations read as

$$\Delta = -\frac{2}{\rho}(\sigma_{12}^2 + \underline{\sigma_{11}^2 + \sigma_{22}^2 + \sigma_{11}\sigma_{22}}) - 12\ \mathrm{Kn}_0\frac{\mu}{p}\times\left(\theta\frac{dq_2}{dx_2} + \underline{\frac{5}{2}q_2\frac{d\theta}{dx_2}} - \underline{\theta q_2\frac{d\ln\rho}{dx_2}} + \theta\sigma_{12}\frac{dv_1}{dx_2}\right), \tag{16}$$

$$R_{12} = -\frac{4}{7\rho}(\underline{\sigma_{11}\sigma_{12} + \sigma_{12}\sigma_{22}}) - \frac{12}{5}\mathrm{Kn}_0\frac{\mu}{p}\left(\theta\frac{dq_1}{dx_2} + \underline{q_1\frac{d\theta}{dx_2}} - \underline{\theta q_1\frac{d\ln\rho}{dx_2}} + \underline{\frac{5}{7}\theta(\sigma_{11} + \sigma_{22})\frac{dv_1}{dx_2}}\right), \tag{17}$$

$$R_{22} = -\frac{4}{21\rho}(\sigma_{12}^2 + \underline{\sigma_{22}^2 - 2\sigma_{11}^2 - 2\sigma_{11}\sigma_{22}}) - \frac{16}{5}\mathrm{Kn}_0\frac{\mu}{p}\times\left(\theta\frac{dq_2}{dx_2} + \underline{q_2\frac{d\theta}{dx_2}} - \underline{\theta q_2\frac{d\ln\rho}{dx_2}} + \frac{5}{14}\theta\sigma_{12}\frac{dv_1}{d\tilde{x}_2}\right), \tag{18}$$

$$m_{112} = -2\ \mathrm{Kn}_0\frac{\mu}{p}\left[\frac{\theta}{3}\left(\frac{d\sigma_{11}}{dx_2} - \frac{2}{5}\frac{d\sigma_{22}}{dx_2}\right) - \underline{\frac{\theta}{3}\left(\sigma_{11}\frac{d\ln\rho}{dx_2} - \frac{2}{5}\sigma_{22}\frac{d\ln\rho}{dx_2}\right)} + \frac{16}{75}q_1\frac{dv_1}{dx_2}\right], \tag{19}$$

$$m_{122} = -2\ \mathrm{Kn}_0\frac{\mu}{p}\times\left(\frac{8}{15}\theta\frac{d\sigma_{12}}{dx_2} - \underline{\frac{8}{15}\theta\sigma_{12}\frac{d\ln\rho}{dx_2}} + \underline{\frac{16}{75}q_2\frac{dv_1}{dx_2}}\right), \tag{20}$$

$$m_{222} = -2\ \mathrm{Kn}_0\frac{\mu}{p}\left(\frac{3}{5}\theta\frac{d\sigma_{22}}{dx_2} - \underline{\frac{3}{5}\theta\sigma_{22}\frac{d\ln\rho}{dx_2}} - \frac{4}{25}q_1\frac{dv_1}{dx_2}\right). \tag{21}$$

Here, $\mathrm{Kn}_0 = \mu_0\sqrt{\theta_0}/p_0L$ is the Knudsen number at the reference equilibrium state; to simplify the notation the hat signs that indicate dimensionless variables are not shown. Equations (8) and (9) are the conservation laws for momentum, while Eq. (10) is the energy balance.

The underlined terms indicate those nonlinear terms that will not be considered. All linear terms and all nonlinear terms that are quadratic in σ_{12} and/or dv_1/dx_2 are retained. Indeed, the nonlinear term in the energy balance accounts for viscous heating effects, which we wish to study. Accordingly, all similar terms must be included in the semilinearized equations. For instance, the nonlinear term $q_1(dv_1/dx_2)$, which appears in Eqs. (15) and (21), must be taken into account because Eq. (14) implies that $d\sigma_{12}/dx_2$ is the leading term for q_1. As will be seen, the nonhydrodynamic linear terms lead to Knudsen boundary layers.

After substitution of constitutive relations and semilinearization Eqs. (8)–(15) reduce to the velocity problem,

$$\frac{d\sigma_{12}}{dx_2} = G_1,$$

$$\frac{2}{5}\frac{dq_1}{dx_2} + \frac{dv_1}{dx_2} - \frac{16}{15}\mathrm{Kn}_0\frac{d^2\sigma_{12}}{dx_2^2} = -\frac{1}{\mathrm{Kn}_0}\sigma_{12}, \tag{22}$$

$$\frac{d\sigma_{12}}{d\tilde{x}_2} - \frac{6}{5}\mathrm{Kn}_0\frac{d^2q_1}{dx_2^2} = -\frac{2}{3}\frac{1}{\mathrm{Kn}_0}q_1,$$

the temperature problem,

$$\frac{dq_2}{dx_2} = -\sigma_{12}\frac{dv_1}{dx_2},$$

$$-\frac{6}{5}\sigma_{12}\frac{dv_1}{dx_2} - \frac{6}{5}\mathrm{Kn}_0\frac{d^2\sigma_{22}}{dx_2^2} - \frac{12}{25}\mathrm{Kn}_0^2\frac{d}{dx_2}\left(\frac{d\sigma_{12}}{dx_2}\frac{dv_1}{dx_2}\right) = -\frac{1}{\mathrm{Kn}_0}\sigma_{22}, \tag{23}$$

$$\frac{5}{2}\frac{d\theta}{dx_2} + \frac{d\sigma_{22}}{dx_2} - \frac{13}{7}\sigma_{12}\frac{d\sigma_{12}}{dx_2} - \frac{67}{105}\mathrm{Kn}_0\frac{d\sigma_{12}}{dx_2}\frac{dv_1}{dx_2} + \frac{36}{35}\mathrm{Kn}_0\ \sigma_{12}\frac{d^2v_1}{dx_2^2} = -\frac{2}{3}\frac{1}{\mathrm{Kn}_0}q_2,$$

and the remainder,

$$\frac{8}{5}\sigma_{12}\frac{dv_1}{dx_2} - \frac{2}{3}\mathrm{Kn}_0\frac{d^2\sigma_{11}}{dx_2^2} + \frac{4}{15}\mathrm{Kn}_0\frac{d\sigma_{22}^2}{dx_2^2} + \frac{16}{25}\mathrm{Kn}_0^2\frac{d}{dx_2}\left(\frac{d\sigma_{12}}{dx_2}\frac{dv_1}{dx_2}\right) = -\frac{1}{\mathrm{Kn}_0}\sigma_{11}, \tag{24a}$$

$$\frac{d(\rho+\theta+\sigma_{22})}{dx_2} = 0. \tag{24b}$$

B. The solutions

As categorized above, semilinearization offers splitting of the equations into three subsets. It is obvious from the equations that, despite the one-dimensional setting for the flow, the full two-dimensional set of R13 variables is involved (all variables that do not appear in the equations vanish due to the chosen flow geometries). By choosing a proper ordering, the above set of equations can be solved analytically. After integration, the solutions for the velocity problem are ($\mathbf{C}_1$ to $\mathbf{C}_8$ are constants of integrating)

$$v_1 = \mathbf{C}_4 - \frac{G_1}{2\ \mathrm{Kn}_0}x_2^2 - \frac{\mathbf{C}_1}{\mathrm{Kn}_0}x_2 - \frac{2}{5}q_1, \tag{25}$$

$$\sigma_{12} = \mathbf{C}_1 + G_1 x_2, \tag{26}$$

$$q_1 = -\frac{3G_1\ \mathrm{Kn}_0}{2} + A, \tag{27}$$

with

$$A = \mathbf{C}_2\sinh\left(\frac{\sqrt{5}}{3\ \mathrm{Kn}_0}x_2\right) + \mathbf{C}_3\cosh\left(\frac{\sqrt{5}}{3\ \mathrm{Kn}_0}x_2\right). \tag{28}$$

The solution of the velocity problem can then be used to solve the temperature problem as

$$\theta = \mathbf{C}_8 - \frac{G_1^2}{45\ \mathrm{Kn}_0^2}x_2^4 - \frac{4G_1\mathbf{C}_1}{45\ \mathrm{Kn}_0^2}x_2^3 + \left(\frac{488G_1^2}{525} - \frac{2\mathbf{C}_1^2}{15\ \mathrm{Kn}_0^2}\right)x_2^2 + \left(\frac{976G_1\mathbf{C}_1}{525} - \frac{4\mathbf{C}_5}{15\ \mathrm{Kn}_0}\right)x_2 + \frac{956G_1\ \mathrm{Kn}_0}{375}A + \frac{96\ \mathrm{Kn}_0}{175}\sigma_{12}\frac{dA}{dx_2} - \frac{2}{5}B, \tag{29}$$

$$q_2 = \mathbf{C}_5 + \frac{G_1^2}{3\ \mathrm{Kn}_0}x_2^3 + \frac{G_1\mathbf{C}_1}{\mathrm{Kn}_0}x_2^2 + \frac{\mathbf{C}_1^2}{\mathrm{Kn}_0}x_2 + \frac{2}{5}\sigma_{12}A - \frac{18\ \mathrm{Kn}_0^2\ G_1}{25}\frac{dA}{dx_2}, \tag{30}$$

$$\sigma_{22} = -\frac{84G_1^2\ \mathrm{Kn}_0^2}{25} - \frac{6G_1^2}{5}x_2^2 - \frac{12G_1\mathbf{C}_1}{5}x_2 - \frac{6\mathbf{C}_1^2}{5} - \frac{152G_1\ \mathrm{Kn}_0}{25}A - \frac{36\ \mathrm{Kn}_0}{25}\sigma_{12}\frac{dA}{dx_2} + B, \tag{31}$$

with

$$B = \mathbf{C}_6\cosh\left(\frac{\sqrt{5}}{\sqrt{6}\ \mathrm{Kn}_0}x_2\right) + \mathbf{C}_7\sinh\left(\frac{\sqrt{5}}{\sqrt{6}\ \mathrm{Kn}_0}x_2\right). \tag{32}$$

The functions A and B, Eqs. (28) and (32), describe Knudsen layer contributions to the solutions. Accordingly, the above solutions are superpositions of Knudsen layers (all terms with A and B) and bulk contributions (all other terms). The integrating constants need to be determined from boundary conditions. Mass density can be obtained by integration of Eq. (24b) as $\rho = \mathbf{C}_9 - \theta - \sigma_{22}$ where the constant $\mathbf{C}_9$ follows from the condition of prescribed mass, $\int_{-1/2}^{1/2}\rho dx_2 = 0$.

The Knudsen layers result already from the fully linearized R13 equations[45] and can also be computed from high-order LB methods.[33,34] However, other than the R13 equations, the latter is limited to the isothermal regime, and thus cannot capture the nonlinear coupling between temperature and velocity.

C. Couette flow

For Couette flow symmetry arguments show that $v_1(x_2) = -v_1(-x_2)$, $q_1(x_2) = -q_1(-x_2)$, and thus $\mathbf{C}_3 = \mathbf{C}_4 = 0$. Moreover, the absence of body forces implies $G_1 = 0$. The general solution for the velocity problem reduces to

$$v_1 = -\underline{\frac{\mathbf{C}_1}{\mathrm{Kn}_0}x_2} - \frac{2}{5}q_1, \quad \sigma_{12} = \underline{\mathbf{C}_1},$$
$$q_1 = \mathbf{C}_2 \sinh\left(\frac{\sqrt{5}}{3\ \mathrm{Kn}_0}x_2\right). \tag{33}$$

For the temperature problem, the symmetry of the temperature profile, $\theta(x_2)=\theta(-x_2)$, gives $\mathbf{C}_5=\mathbf{C}_7=0$, so that

$$\theta = \underline{\mathbf{C}_8 - \frac{2\mathbf{C}_1^2}{15\ \mathrm{Kn}_0^2}x_2^2} + \frac{32\mathbf{C}_2}{35\sqrt{5}}\sigma_{12}\cosh\left(\frac{\sqrt{5}}{3\ \mathrm{Kn}_0}x_2\right) - \frac{2\mathbf{C}_6}{5}\cosh\left(\frac{\sqrt{5}}{\sqrt{6}\ \mathrm{Kn}_0}x_2\right),$$
$$\sigma_{22} = -\frac{6\mathbf{C}_1^2}{5} - \frac{12\mathbf{C}_2}{5\sqrt{5}}\sigma_{12}\cosh\left(\frac{\sqrt{5}}{3\ \mathrm{Kn}_0}x_2\right) + \mathbf{C}_6\cosh\left(\frac{\sqrt{5}}{\sqrt{6}\ \mathrm{Kn}_0}x_2\right), \tag{34}$$
$$q_2 = \underline{\frac{\mathbf{C}_1^2}{\mathrm{Kn}_0}x_2} + \frac{2\mathbf{C}_2}{5}\sigma_{12}\sinh\left(\frac{\sqrt{5}}{3\ \mathrm{Kn}_0}x_2\right).$$

Note that for Couette flow the momentum balance yields constant shear stress, $\sigma_{12}=\mathbf{C}_1$. The constants $\mathbf{C}_1$ and $\mathbf{C}_8$ are related to velocity slip and temperature jump. The constants will be determined from boundary conditions below.

Only the underlined terms in Eqs. (33) and (34) would be present in classical hydrodynamics as solutions of the Navier–Stokes–Fourier equations. All other terms, including the hyperbolic sine and cosine functions of the Knudsen boundary layers, describe rarefaction effects. The heat flux parallel to the walls, q_1, is just a Knudsen boundary layer, while the normal stress σ_{22} is a superposition of a constant bulk term,[41] $-6\mathbf{C}_1^2/5$, and a Knudsen layer. In classical hydrodynamics, the temperature profile is parabolic; the R13 equations add Knudsen layer contributions.

D. Poiseuille flow

Velocity and temperature distributions in force-driven Poiseuille flow are both symmetric, so that $\mathbf{C}_1=\mathbf{C}_2=\mathbf{C}_5=\mathbf{C}_7=0$. Consequently, the solutions for Poiseuille flow read as

$$v_1 = \underline{\mathbf{C}_4 - \frac{G_1}{2\ \mathrm{Kn}_0}x_2^2} - \frac{2}{5}q_1, \quad \sigma_{12} = \underline{G_1 x_2},$$
$$q_1 = -\frac{3G_1\ \mathrm{Kn}_0}{2} + \mathbf{C}_3\cosh\left(\frac{\sqrt{5}}{3\ \mathrm{Kn}_0}x_2\right) \tag{35}$$

and

$$\theta = \underline{\mathbf{C}_8 - \frac{G_1^2}{45\ \mathrm{Kn}_0^2}x_2^4} + \frac{488G_1^2}{525}x_2^2 + \frac{32\mathbf{C}_3}{35\sqrt{5}}\sigma_{12}\sinh\left(\frac{\sqrt{5}}{3\ \mathrm{Kn}_0}x_2\right) + \frac{956G_1\ \mathrm{Kn}_0\ \mathbf{C}_3}{375}\cosh\left(\frac{\sqrt{5}}{3\ \mathrm{Kn}_0}x_2\right) - \frac{2\mathbf{C}_6}{5}\cosh\left(\frac{\sqrt{5}}{\sqrt{6}\ \mathrm{Kn}_0}x_2\right),$$
$$q_2 = \underline{\frac{G_1^2}{3\ \mathrm{Kn}_0}x_2^3} + \frac{2\mathbf{C}_3}{5}\sigma_{12}\cosh\left(\frac{\sqrt{5}}{3\ \mathrm{Kn}_0}x_2\right) - \frac{6G_1\ \mathrm{Kn}_0\ \mathbf{C}_3}{5\sqrt{5}}\sinh\left(\frac{\sqrt{5}}{3\ \mathrm{Kn}_0}x_2\right), \tag{36}$$
$$\sigma_{22} = -\frac{84G_1^2\ \mathrm{Kn}_0^2}{25} - \frac{6G_1^2}{5}x_2^2 - \frac{12\mathbf{C}_3}{5\sqrt{5}}\sigma_{12}\sinh\left(\frac{\sqrt{5}}{3\ \mathrm{Kn}_0}x_2\right) - \frac{152G_1\ \mathrm{Kn}_0\ \mathbf{C}_3}{25}\cosh\left(\frac{\sqrt{5}}{3\ \mathrm{Kn}_0}x_2\right) + \mathbf{C}_6\cosh\left(\frac{\sqrt{5}}{\sqrt{6}\ \mathrm{Kn}_0}x_2\right).$$

In this case, σ_{12} is a linear function of x_2. Velocity slip and temperature jump will affect the values of the constants $\mathbf{C}_4$ and $\mathbf{C}_8$, respectively.

Again, the underlined terms denote the Navier–Stokes–Fourier solutions. All other terms, including the hyperbolic sine and cosine functions of the Knudsen layers, describe rarefaction effects. In Poiseuille flow (like Couette flow) neither q_1 nor σ_{22} include Navier–Stokes–Fourier terms; both are superpositions of bulk solutions and Knudsen boundary layers. The temperature profile of classical hydrodynamics is given by the fourth power of x_2; the R13 equations correct this value by adding a quadratic term in x_2 and Knudsen layer contributions.

V. BOUNDARY CONDITIONS

All extended systems that go beyond the Navier–Stokes–Fourier require additional boundary conditions. For the Burnett equations higher-order gradients of the hydrodynamic variables must be prescribed. For Grad-type moment methods, on the other hand, the challenge is the construction of boundary conditions for higher-order moments. Since ill posed boundary conditions can lead to unphysical results, great care must be taken in deriving and implementing boundary conditions for extended models.

In the present study, we use the kinetic boundary conditions for the R13 system,[44] which were obtained based on Maxwell's boundary condition for the Boltzmann equation.[47] The boundary conditions link the moments of the gas near the wall to the wall velocity v_1^W and wall temperature θ_W. Extensive discussions on the approach are available in the literature.[1,35,43,44,47,48] Derivation of the required boundary

conditions for the high-order moments in the R13 system is performed[44] by using the velocity distribution function of Grad's 26-moment system, with the R13 constitutive equations, Eq. (5).

In the solutions, Eqs. (33)–(36), each problem includes four unknown constants of integration. Hence, four boundary conditions at one wall are required to evaluate these constants, while the boundary conditions for the other wall are guaranteed due to symmetry. Note that in the absence of Knudsen boundary layers, i.e., in classical hydrodynamics, the number of required boundary conditions is reduced to 2 at one wall, while the integrating constants in Eqs. (28) and (32) are zero.

To be consistent with the semilinearized R13 equations, we restrict ourselves to semilinearized boundary conditions which in dimensionless form read as

$$\sigma_{12} = -\beta_1\sqrt{\frac{2}{\pi}}\left(\mathcal{V} + \frac{1}{5}q_1 + \frac{1}{2}m_{122}\right)n_2,$$

$$q_2 = -\beta_2\sqrt{\frac{2}{\pi}}\left(2\mathcal{T} - \underline{\frac{1}{2}\mathcal{V}^2} + \frac{1}{2}\sigma_{22} + \frac{1}{15}\Delta + \frac{5}{28}R_{22}\right)n_2,$$

$$m_{222} = \beta_3\sqrt{\frac{2}{\pi}}\left(\frac{2}{5}\mathcal{T} - \underline{\frac{3}{5}\mathcal{V}^2} - \frac{7}{5}\sigma_{22} + \frac{1}{75}\Delta - \frac{1}{14}R_{22}\right)n_2, \quad (37)$$

$$R_{12} = \beta_4\sqrt{\frac{2}{\pi}}\left(\mathcal{V} - \frac{11}{5}q_1 - \frac{1}{2}m_{122}\right)n_2,$$

$$m_{112} - m_{233} = -\beta_5\sqrt{\frac{2}{\pi}}\left(\frac{1}{14}(R_{11} - R_{33}) + \sigma_{11} - \sigma_{33} - \underline{\mathcal{V}^2}\right)n_2,$$

with the abbreviations

$$\mathcal{P} = 1 + \rho + \theta + \tfrac{1}{2}\sigma_{22} - \tfrac{1}{120}\Delta - \tfrac{1}{28}R_{22},$$
$$\mathcal{V} = v_1 - v_1^W, \quad \mathcal{T} = \theta - \theta_W, \quad \beta_i = \frac{\chi_i}{2 - \chi_i}, \quad (38)$$

where all quantities have to be evaluated at the left wall. Here, n_2 is the normal vector of the left wall pointing toward the gas, $\mathbf{n}=\{0,1,0\}$, see Fig. 1. The sub-/superscript W refers to wall properties; thus, $\mathcal{V}=v_1-v_1^W$ and $\mathcal{T}=\theta-\theta_W$ denote dimensionless velocity slip and temperature jump. The first equation in Eq. (37) is the slip condition that links the slip velocity $\mathcal{V}$ to the tangential components of stress tensor, heat-flux vector, and moment m_{ijk}. Similarly, the second equation gives the temperature jump $\mathcal{T}$ in terms of normal components of heat-flux vector, stress tensor, and moment R_{ij}. Surface accommodation factors in the Maxwell model are presented by $0\le\chi_i\le1$, where $\chi=0$ and 1 denote no accommodation (specular reflection of gas particles on the wall) and full accommodation (thermalization of gas particles on the wall) scenarios, respectively. The coefficients $0\le\beta_i\le1$ are modified accommodation factors that can be used for fitting. In the context of the present paper, however, we shall only consider full accommodation where $\chi_i=1$, and thus $\beta_i=1$ for all i.

The only nonlinear terms left in the above boundary conditions are the underlined quadratic terms in velocity slip (shear). These nonlinear terms correct the temperature jump and provide a better match with DSMC results.

For completeness of the discussion, we mention that the semilinearized R13 equations require the same number of boundary conditions as the linearized R13 equations, as given above. The fully nonlinear R13 equations, however, require additional boundary conditions for higher moments which can be obtained from asymptotic analysis of the equations.[44]

The classical second-order slip and jump boundary conditions[19–21] can be extracted from Eq. (37) by expansion in the Knudsen number.[49]

VI. RESULTS

In this section, the results of analytical solutions for semilinearized Couette and force-driven Poiseuille flows are illustrated and compared to DSMC simulations. For the same problems, numerical solutions for fully nonlinear equations were recently published.[44]

Figure 2 shows the dimensionless R13 solutions for the velocity and temperature problems for Couette flow. The obtained results are compared to DSMC simulations at Kn $=0.05$, 0.1, and 0.5 for argon. The DSMC results are obtained for Maxwell molecules based on Bird's code,[22] where at standard conditions (101325 Pa and 0 °C) molecular mass, viscosity, and viscosity exponent for argon read as $m=66.3\times10^{-27}$ kg, $\mu_0=2.117\times10^{-5}$ N s m^{-2}, and $\omega=0.81$. The walls move with $v_W=\pm100$ m/s ($\tilde{v}_W=\pm0.4195$) at temperature 273 K ($\tilde{\theta}_W=1$). As depicted, for small Knudsen numbers—where the case is close to classical hydrodynamics—the profiles are in good agreement with DSMC results. For larger Knudsen numbers, where the rarefaction effects are strong, some difference to the DSMC results is observed, especially at the boundaries. Our analytical approach treats viscosity independent of temperature. Indeed, dependence of viscosity on temperature covers a portion of nonlinear effects, which are excluded in the presented calculations. This can be addressed as the main reason for differences between the DSMC and analytical results. The tangential heat flux q_1 and the normal stress σ_{22}, which both vanish in classical hydrodynamics, are predicted with acceptable accuracy.

Figure 3 shows the results for semilinearized Poiseuille flow. The dimensionless external force is $\tilde{G}_1=0.2355$, and the walls are stationary at 273 K ($\tilde{\theta}_W=1$). The results for Kn$=0.072$ are compared to DSMC simulations.[11,12]

An interesting phenomenon observed in force-driven Poiseuille flow is the formation of a characteristic dip in the temperature profile, see the profile for θ in Fig. 3. This minimum was first reported by Tij and Santos[7] who did not include Knudsen boundary layers in their solution. The analytical solution for θ in Eq. (36) lucidly describes the dip as a result of competition between the bulk contributions, $-G_1^2/(45\ \mathrm{Kn}_0^2)x_2^4$ and $\frac{488}{525}G_1^2x_2^2$, while the Knudsen boundary layers contribute to the boundary curvature.

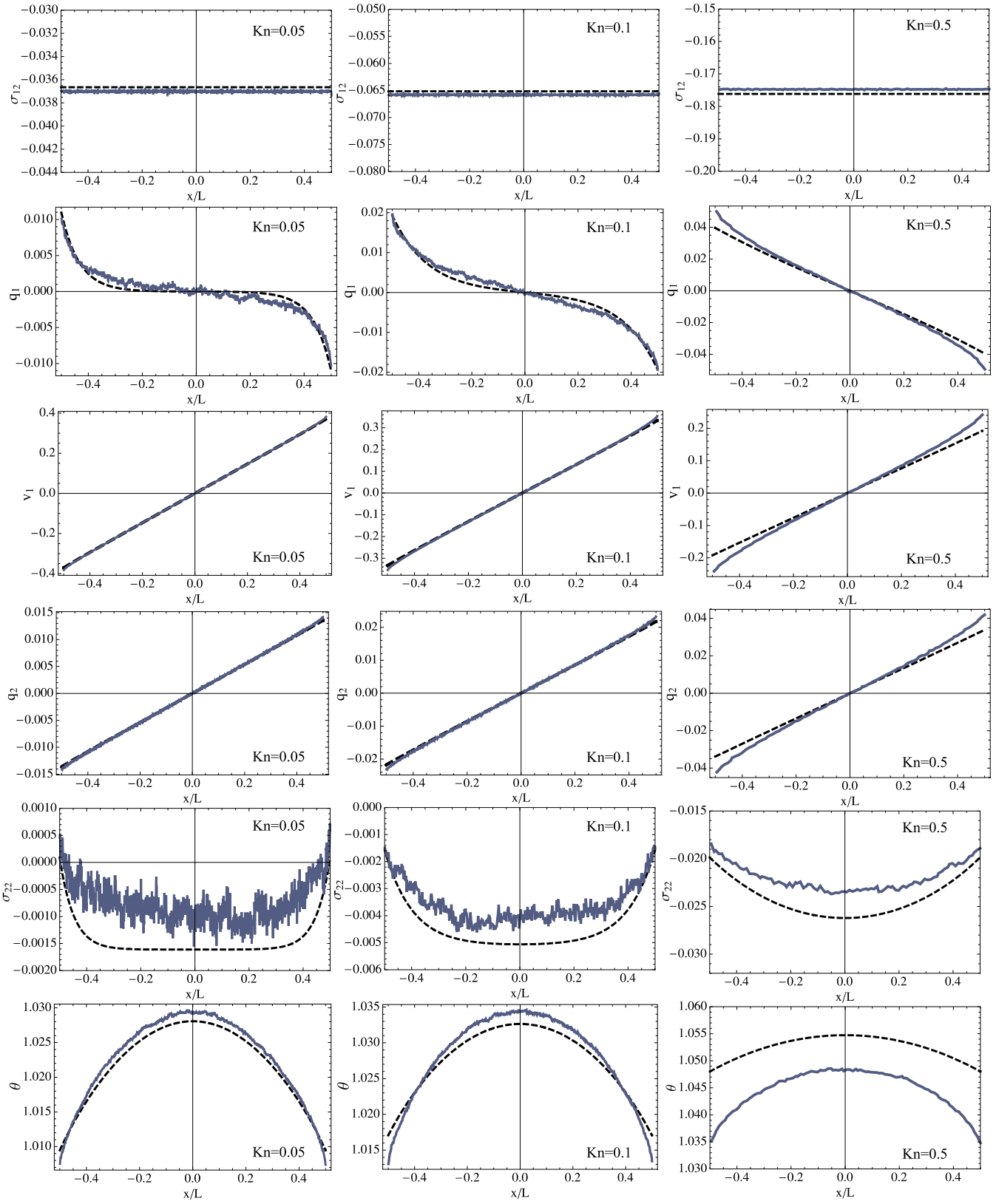

FIG. 2. (Color online) Dimensionless profiles across the channel for Couette flow with argon. Wall temperature and velocities are 273 K and ±100 m/s. Comparison between semilinear R13 (dashed lines) and DSMC (solid lines).

In Fig. 4, the dashed line presents the superposition of the bulk terms and the temperature jump for Kn=0.072 and $\widetilde{G}_1$=0.2355. Moreover, the solid line shows the complete solution, which includes the Knudsen boundary layers. As expected, the Knudsen layers strongly affect the temperature (and also other flow parameters) distribution near the boundaries. At small Knudsen numbers, the effect of the Knudsen layers on the temperature dip is negligible. Inclusion of more

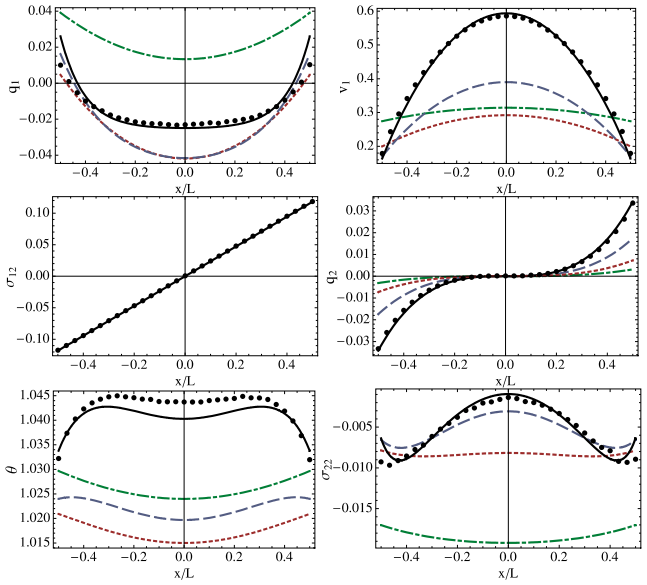

FIG. 3. (Color online) Force-driven Poiseuille flow with dimensionless force $\tilde{\mathbf{G}}=\{0.2355,0,0\}$. Profiles are computed for Kn=0.072 (solid line), 0.15 (dashed line), 0.4 (dotted line), and 1.0 (dashed-dotted line). For Kn =0.072 comparison with DSMC simulation (circles) is presented.

nonlinear terms might change finer details of the curve, such that better agreement with DSMC results is achieved.[7]

It is worth to emphasize on the minimal computational effort required in this approach to predict the temperature dip compared to the others which require numerical tools.[12,44] Recently, a new multistep Bhatnagar-Gross-Krook (BGK) collision operator was proposed[46] which captures the effects of Knudsen boundary layers but requires complicated numerical solutions.

The velocity profiles show a decrease in flow velocity in the middle of the channel as the Knudsen number increases, but the slip is increasing due to a decrease in friction. That is why the velocity curve for Kn=1 lies above the curve of Kn=0.4. Accordingly, the mass flow rate $J=\int_{-1/2}^{1/2} v_1 dx_2$ as a function of Knudsen number exhibits a minimum around Kn=1, which is known as the Knudsen minimum.[17] In Fig. 5 the relative mass flow rate $\hat{J}=J/(\sqrt{2}G)$ is plotted as a function of the modified Knudsen number $\widehat{\mathrm{Kn}}=4\sqrt{2}\ \mathrm{Kn}/5$ for

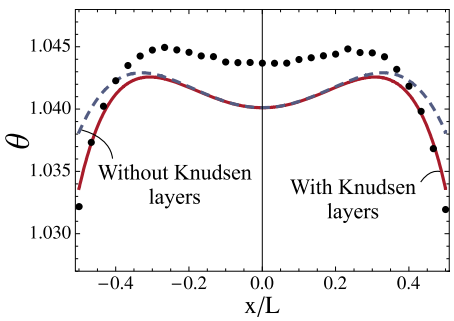

FIG. 4. (Color online) Influence of Knudsen boundary layers on temperature profile in force-driven Poiseuille flow. The dashed line represents the superposition of bulk solutions and the temperature jump. The solid line is the full solution including the Knudsen boundary layers. Dots indicate DSMC simulation for Kn=0.072 and $\tilde{G}_1=0.2355$.

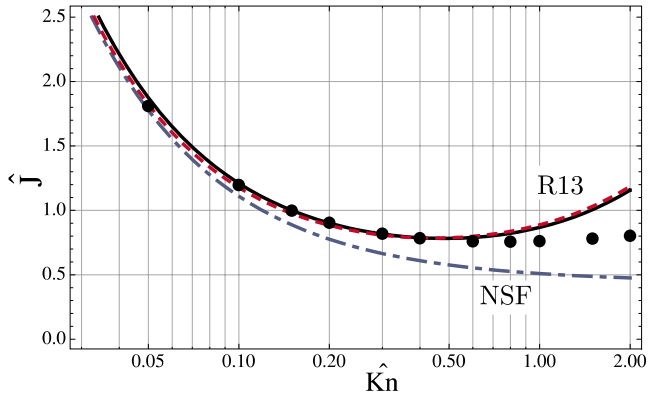

FIG. 5. (Color online) Relative mass flow rate for force-driven Poiseuille flow. Navier–Stokes–Fourier and R13 are compared to linearized Boltzmann equation (dots).

linear R13,[45] semilinear R13, Navier–Stokes–Fourier, and linearized Boltzmann equation.[16] The analytical equation for J in the linear case is available in Ref. 45; however, for the semilinear case discussed above the analytical solution for J is rather bulky to be presented. Figure 5 shows that both the linear and the semilinear R13 systems predict the Knudsen minimum around $\widehat{\mathrm{Kn}}=0.5$, while the Navier–Stokes–Fourier system fails to capture this minimum. It was shown that the DSMC approach is able to predict the Knudsen minimum with the same accuracy as the linearized Boltzmann equation.[34] The plot for the semilinear case is obtained for $G=0.2355$, while the results of linearized Boltzmann equation correspond to small body force. As expected, by decreasing the body force the curves for linear and semilinear R13 become identical. However, for large body forces, the position of the minimum shifts to slightly larger values for $\widehat{\mathrm{Kn}}$. Thus, we conclude that in the semilinearized system the body force affects the Knudsen minimum.

The presented results are obtained for fully diffusive boundary conditions, i.e., all accommodation coefficients are set to unity, $\beta_i=1$. Based on our observations for Poiseuille flow, a slight decrease in $\beta_2(=0.85)$ shifts the temperature dip toward a perfect match with the DSMC data; however, this results in some deviations at the boundaries. Moreover, setting $\beta_3=0.4$ and $\beta_4=0.7$ efficiently corrects the values of σ_{22} and q_1 at the boundaries. These adjustments of the (modified) accommodation coefficients β_i impose almost no change to the other profiles, and simultaneous application of these adjustments leads to a remarkable consistency with the DSMC data.

In this context we note that Knudsen layers are not subject to expansion procedures based on the Knudsen number. The true Knudsen layers are superpositions of many layers of the types (28) and (32), which result from taking a large number of moments into account.[50] Adjustment of the β_i provides a means to approximately account for the additional Knudsen layers. However, presently we refrain from suggesting specific values for adjusting the β_i since this would require a large number of tests for different flow problems and Knudsen numbers.

VII. CONCLUSIONS

We considered a semilinearized version of the R13-moment equations, where the included nonlinear terms all correspond to shear stress and shear rate. Shear flow between two parallel plates is employed as a generic model for microchannel flows. As discussed, semilinearization reduces the equations, so that analytical solutions can be obtained which accurately predict rarefaction effects such as velocity slip, temperature jump, characteristic temperature dip, and formation of Knudsen boundary layers. A distinctive feature of the presented approach is the minimal computational effort required to obtain the solutions compared to the nonlinear case.

The outstanding accuracy of the results obtained here and those in Ref. 44 confirms the physical and mathematical consistency of the R13 equations and the proposed boundary conditions. This is an encouraging result which motivates further investigation in order to extend boundary conditions for other flow configurations, which are common in engineering designs.

ACKNOWLEDGMENTS

Support by the Natural Sciences and Engineering Research Council (NSERC) and the European Science Foundation (ESF) is gratefully acknowledged. The authors thank Dr. Kun Xu (Hong Kong) for providing the DSMC data for Poiseuille flow.

APPENDIX: DIMENSIONLESS PARAMETERS

The reference equilibrium state is defined by $\{\rho_0, \theta_0, v_i^0 = 0\}$, and the dimensionless independent variables $\tilde{\mathbf{x}}$ and $\tilde{t}$ are defined as

$$\tilde{x}_i = \frac{x_i}{L} \quad \text{and} \quad \tilde{t} = \frac{t}{\frac{L}{\sqrt{\theta_0}}}, \tag{A1}$$

where L and $\sqrt{\theta_0}$ denote macroscopic length scale and thermal speed at reference state, respectively. Dimensionless density and temperature are defined as deviations from the reference state,

$$\tilde{\rho} = \frac{\rho - \rho_0}{\rho_0} \quad \text{and} \quad \tilde{\theta} = \frac{\theta - \theta_0}{\theta_0}. \tag{A2}$$

Accordingly,

$$p = \rho\theta = \rho_0(1+\tilde{\rho})\theta_0(1+\tilde{\theta}) = p_0(1+\tilde{\rho}+\tilde{\theta}), \quad \text{where } \tilde{\rho}\tilde{\theta} \simeq 0. \tag{A3}$$

The other dimensionless variables are

$$\tilde{G}_i = \frac{L}{\theta_0} G_i, \quad \tilde{v}_i = \frac{v_i}{\sqrt{\theta_0}}, \quad \tilde{\sigma}_{ij} = \frac{\sigma_{ij}}{\rho_0\theta_0}, \quad \tilde{q}_i = \frac{q_i}{\rho_0\sqrt{\theta_0}^3},$$
$$\tilde{\Delta} = \frac{\Delta}{\rho_0\theta_0^2}, \quad \tilde{R}_{ij} = \frac{R_{ij}}{\rho_0\theta_0^2}, \quad \tilde{m}_{ijk} = \frac{m_{ijk}}{\rho_0\sqrt{\theta_0}^3}. \tag{A4}$$

Moreover, the dimensionless viscosity $\tilde{\mu}$, which is a property of the fluid, is defined as

$$\tilde{\mu} = \frac{\mu}{\mu_0}, \quad \text{where } \mu_0 = \mu(\theta_0). \tag{A5}$$

In the governing equations, wherever we have viscosity, the dimensionless equations will include the reference Knudsen number Kn_0,

$$\mathrm{Kn}_0 = \frac{\mu_0\sqrt{\theta_0}}{p_0 L}. \tag{A6}$$

[1] H. Struchtrup, *Macroscopic Transport Equations for Rarefied Gas Flows* (Springer, New York, 2005).
[2] A. Baranyai, D. J. Evans, and P. J. Daivis, "Isothermal shear-induced heat-flow," Phys. Rev. A **46**, 7593 (1992).
[3] B. D. Todd and D. J. Evans, "The heat-flux vector for highly inhomogeneous nonequilibrium fluids in very narrow pores," J. Chem. Phys. **103**, 9804 (1995).
[4] B. D. Todd and D. J. Evans, "Temperature profile for Poiseuille flow," Phys. Rev. E **55**, 2800 (1997).
[5] F. J. Uribe and A. L. Garcia, "Burnett description for plane Poiseuille flow," Phys. Rev. E **60**, 4063 (1999).
[6] K. Aoki, S. Takata, and T. Nakanishi, "Poiseuille type flow of a rarefied gas between two parallel plates driven by a uniform external force," Phys. Rev. E **65**, 026315 (2002).
[7] M. Tij and A. Santos, "Perturbation analysis of a stationary nonequilibrium flow generated by an external force," J. Stat. Phys. **76**, 1399 (1994).
[8] M. Malek Mansour, F. Baras, and A. L. Garcia, "On the validity of hydrodynamics in plane Poiseuille flows," Physica A **240**, 255 (1997).
[9] M. Tij, M. Sabbane, and A. Santos, "Nonlinear Poiseuille flow in a gas," Phys. Fluids **10**, 1021 (1998).
[10] M. Alaoui and A. Santos, "Poiseuille flow driven by an external force," Phys. Fluids A **4**, 1273 (1992).
[11] Y. Zheng, A. L. Garcia, and B. J. Alder, "Comparison of kinetic theory and hydrodynamics for Poiseuille flow," J. Stat. Phys. **109**, 495 (2002).
[12] K. Xu, "Super-Burnett solutions for Poiseuille flow," Phys. Fluids **15**, 2077 (2003).
[13] K. Xu and Z. Li, "Microchannel flow in the slip regime: Gas-kinetic BGK–Burnett solutions," J. Fluid Mech. **513**, 87 (2004).
[14] Y. Sone, *Kinetic Theory and Fluid Dynamics* (Birkhäuser, Boston, 2002).
[15] D. Risso and P. Cordero, "Generalized hydrodynamics for a Poiseuille flow: Theory and simulations," Phys. Rev. E **58**, 546 (1998).
[16] T. Ohwada, Y. Sone, and K. Aoki, "Numerical analysis of the Poiseuille and thermal transpiration flows between two parallel plates on the basis of the Boltzmann equation for hard-sphere molecules," Phys. Fluids A **1**, 2042 (1989).
[17] M. Knudsen, "Die Gesetze der Molekularströmung und der inneren Reibungsströmung der Gase durch Röhren," Ann. Phys. **333**, 75 (1909).
[18] K. A. Hickey and S. K. Loyalka, "Plane Poiseuille flow: Rigid sphere gas," J. Vac. Sci. Technol. A **8**, 957 (1990).
[19] R. G. Deissler, "An analysis of second order slip flow and temperature jump boundary conditions for rarefied gases," Int. J. Heat Mass Transfer **7**, 681 (1964).
[20] N. G. Hadjiconstantinou, "Comment on Cercignani's second-order slip coefficient," Phys. Fluids **15**, 2352 (2003).
[21] D. A. Lockerby, J. M. Reese, D. R. Emerson, and R. W. Barber, "Velocity boundary condition at solid walls in rarefied gas calculations," Phys. Rev. E **70**, 017303 (2004).
[22] G. A. Bird, *Molecular Gas Dynamics and the Direct Simulation of Gas Flows* (Oxford University Press, New York, 1998).

[23]S. Succi, *The Lattice Boltzmann Equation* (Oxford University Press, New York, 2001).
[24]D. A. Wolf-Gladrow, *Lattice Gas Cellular Automata and Lattice Boltzmann Models* (Springer, New York, 2000).
[25]S. Chapman and T. G. Cowling, *The Mathematical Theory of Non-uniform Gases* (Cambridge University Press, Cambridge, 1970).
[26]A. V. Bobylev, "The Chapman-Enskog and Grad methods for solving the Boltzmann equation," Sov. Phys. Dokl. **27**, 29 (1982).
[27]P. Rosenau, "Extending hydrodynamics via the regularization of the Chapman-Enskog expansion," Phys. Rev. A **40**, 7193 (1989).
[28]X. Zhong, R. W. MacCormack, and D. R. Chapman, "Stabilization of the Burnett equations and applications to hypersonic flows," AIAA J. **31**, 1036 (1993).
[29]S. Jin and M. Slemrod, "Regularization of the Burnett equations via relaxation," J. Stat. Phys. **103**, 1009 (2001).
[30]I. Müller, D. Reitebuch, and W. Weiss, "Extended thermodynamics—Consistent in order of magnitude," Continuum Mech. Thermodyn. **15**, 113 (2003).
[31]A. V. Bobylev, "Instabilities in the Chapman-Enskog expansion and hyperbolic Burnett equations," J. Stat. Phys. **124**, 371 (2006).
[32]L. H. Söderholm, "Hybrid Burnett equations: A new method of stabilizing," Transp. Theory Stat. Phys. **36**, 495 (2007).
[33]S. Ansumali, I. V. Karlin, S. Arcidiacono, A. Abbas, and N. I. Prasianakis, "Hydrodynamics beyond Navier-Stokes: Exact solution to the lattice Boltzmann hierarchy," Phys. Rev. Lett. **98**, 124502 (2007).
[34]S. H. Kim and H. Pitsch, "Analytical solution for a higher-order lattice Boltzmann method: Slip velocity and Knudsen layer," Phys. Rev. E **78**, 016702 (2008).
[35]H. Grad, "On the kinetic theory of rarefied gases," Commun. Pure Appl. Math. **2**, 325 (1949).
[36]H. Grad, in *Handbuch der Physik*, edited by S. Flügge (Springer, Berlin, 1958), Vol. 12.
[37]I. V. Karlin, A. N. Gorban, G. Dukek, and T. F. Nonnenmacher, "Dynamic correction to moment approximations," Phys. Rev. E **57**, 1668 (1998).
[38]H. Struchtrup and M. Torrilhon, "Regularization of Grad's 13-moment equations: Derivation and linear analysis," Phys. Fluids **15**, 2668 (2003).
[39]H. Struchtrup, "Stable transport equations for rarefied gases at high orders in the Knudsen number," Phys. Fluids **16**, 3921 (2004).
[40]M. Torrilhon and H. Struchtrup, "Regularized 13-moment-equations: Shock structure calculations and comparison to Burnett models," J. Fluid Mech. **513**, 171 (2004).
[41]H. Struchtrup and T. Thatcher, "Bulk equations and Knudsen layers for the regularized 13 moment equations," Continuum Mech. Thermodyn. **19**, 177 (2007).
[42]D. Lockerby and J. Reese, "On the modelling of isothermal gas flows at the microscale," J. Fluid Mech. **604**, 235 (2008).
[43]X. J. Gu and D. R. Emerson, "A computational strategy for the regularized 13-moment equations with enhanced wall-boundary conditions," J. Comput. Phys. **225**, 263 (2007).
[44]M. Torrilhon and H. Struchtrup, "Boundary conditions for regularized 13-moment-equations for micro-channel-flows," J. Comput. Phys. **227**, 1982 (2008).
[45]H. Struchtrup and M. Torrilhon, "H theorem, regularization, and boundary conditions for linearized 13-moment equations," Phys. Rev. Lett. **99**, 014502 (2007).
[46]K. Xu, "A generalized Bhatnager–Gross–Kook model for nonequilibrium flows," Phys. Fluids **20**, 026101 (2008).
[47]J. C. Maxwell, "On stresses in rarefied gases arising from inequalities of temperature," Philos. Trans. R. Soc. London **170**, 231 (1879).
[48]H. Struchtrup and W. Weiss, "Temperature jump and velocity slip in the moment method," Continuum Mech. Thermodyn. **12**, 1 (2000).
[49]H. Struchtrup and M. Torrilhon, "High order effects in rarefied channel flows," Phys. Rev. E **78**, 046301 (2008).
[50]H. Struchtrup, "Linear kinetic heat transfer: Moment equations, boundary conditions, and Knudsen layers," Physica A **387**, 1750 (2008).